Supporting Information

Imaging Patterns in Model Lipid Membranes Through the use of BODIPY Based Molecular Rotors

Michael R. Dent,[1] *Ismael López-Duarte*,[1] *Callum J. Dickson*,[1] *Niall Geoghegan*,[2] *Jon M. Cooper*,[2] *Ian R. Gould*,[1] *Rob Krams*,[3] *James A. Bull*,[1] *Nicholas J. Brooks*[1]* *and Marina K. Kuimova*[1]*

1 Department of Chemistry, Imperial College London, Exhibition Road, London, SW7 2AZ, United Kingdom

2 Division of Biomedical Engineering, School of Engineering, University of Glasgow, Oakfield Avenue, Glasgow, G12 8LT, United Kingdom

3 Department of Bioengineering Royal School of Mines Building, Imperial College London, Exhibition Road, London, SW7 2AZ, United Kingdom

Correspondence to: m.kuimova@imperial.ac.uk; nicholas.brooks@imperial.ac.uk

Table of Contents for Supporting Information

(1) Molecular Dynamics Simulations

[1] Simulation parameters. The three dyes under study, C_{10}-BODIPY, Chol-BODIPY and Charge-BODIPY++ were parameterized using the Antechamber tool in the AMBER suite,[1] allowing the assignment of GAFF atom types and parameters.[2] Rather than use the AM1-BCC charges automatically assigned, the two-stage RESP charge fitting procedure was used to assign partial charges calculated at the HF/6-31G* level in gas phase to the three dye molecules.[3,4] DPPC and DOPC lipid molecules were modelled using the recently developed Lipid14 force field[5] whilst water was represented by the TIP3P potential.[6] In all cases, bilayers contained 128 lipid molecules (64 per leaflet). The DOPC bilayer was solvated with 70 waters per lipid and the gel phase DPPC bilayer with 30 waters per lipid.

The following simulations were then performed: diffusion of the three dyes within a DOPC membrane over the temperature range 283, 293, 303, 313, 323 and 333 K; and the preferred position and diffusion of C_{10}-BODIPY in a DPPC membrane at 293 K only, meaning the DPPC membrane was in a gel state.

[2] System setup. To construct initial coordinates for each of the three dyes inside a DOPC membrane, each dye was placed in the water phase above a DOPC bilayer and the system simulated for 100 ns at 303 K, during which time each dye diffused into the membrane. To construct initial coordinates for C_{10}-BODIPY inside a gel phase DPPC bilayer, the dye was positioned within the membrane at two locations: lying along the membrane normal with carbon tail pointing towards the membrane core, and lying along the membrane plane positioned in the centre of the membrane.

[3] Equilibration procedure. The full system was minimized for 10000 steps, of which the first 5000 steps used the steepest descent method and the remaining steps used the conjugate gradient method.[7]

The system was then heated from 0 K to 100 K using Langevin dynamics[8] for 5 ps at constant volume, with weak restraints on the dye and the lipid (force constant 10 kcal mol^{-1} $Å^{-2}$).

Following this, the volume was allowed to change freely and the temperature increased to the

desired temperature with a Langevin collision frequency of γ = 1.0 ps^{-1}, and anisotropic Berendsen regulation[9] (1 atm) with a time constant of 2 ps for 100 ps. The same weak restraint of 10 kcal mol^{-1} $Å^{-2}$ was maintained on the dye and lipid molecules.

[4] Production runs. Constant pressure and constant temperature (NPT) runs were performed using the AMBER 12 package.[1] The GPU implementation of the AMBER 12 code was used to run the simulations on NVIDIA GPU cards.[1,10-12] Three dimensional periodic boundary conditions with the usual minimum image convention were employed. Bonds involving hydrogen were constrained using the SHAKE algorithm,[13] allowing a 2 fs time step. Structural data was recorded every 10 ps. PME was used to treat all electrostatic interactions with a real space cut-off of 10 Å. A long-range analytical dispersion correction was applied to the energy and pressure. All simulations were performed at constant pressure of 1 atm and constant target temperature. Temperature was controlled by the Langevin thermostat,[8] with a collision frequency of γ = 1.0 ps^{-1}. Pressure was regulated by the anisotropic Berendsen method[9] (1 atm) with a pressure relaxation time of 1.0 ps.

Each system was simulated for 100 ns. Diffusion analysis was performed with CPPTRAJ.[14] The mean-square-displacement (MSD) of each dye was calculated after the artificial centre-of-mass drift of the monolayer in which the dye resides was first removed.[15] The MSD was time averaged using 5 ns windows using time origins separated by 100 ps. The slope of the linear 2-5 ns region of the resulting MSD versus time curve was then fitted to obtain a diffusion coefficient using the Einstein relation.

RESULTS

Dye diffusion results. The resulting diffusion coefficients for each of the three dyes in a DOPC membrane over the temperature range 283-333 K are given in Table S1 and plotted in Fig. S1. Electron density profiles of the three systems are shown in Fig. S2. The three dyes retained a similar orientation during the course of the 100 ns simulations.

Table S1 – Simulation diffusion coefficient values for each of the three dyes in a DOPC membrane simulation for 100 ns over a temperature range 283 – 303 K.

Temperature (K)	**Simulation diffusion coefficient (10^{-8} cm^2s^{-1})**		
	Rotor 1	**Rotor 2**	**Rotor 3**
283	5.39	6.72	3.37
293	10.22	7.52	7.06
303	13.59	12.68	10.49
313	16.45	14.39	12.20
323	20.72	15.53	12.20
333	22.67	21.61	18.74

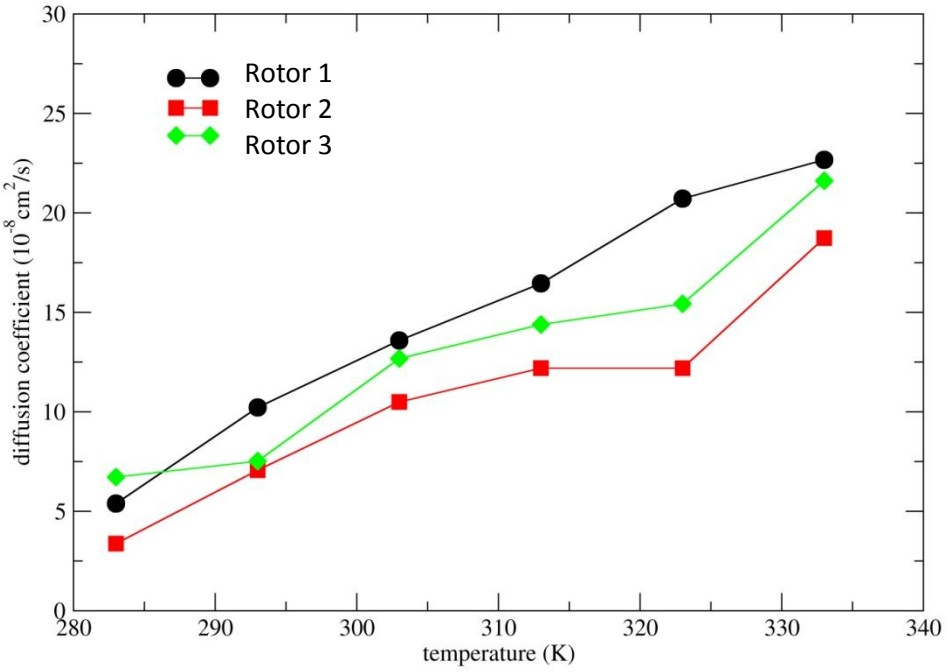

Fig. S1 Plot of simulation diffusion coefficient values for each of the three dyes in a DOPC membrane simulation for 100 ns over a temperature range 283 – 303 K.

a)

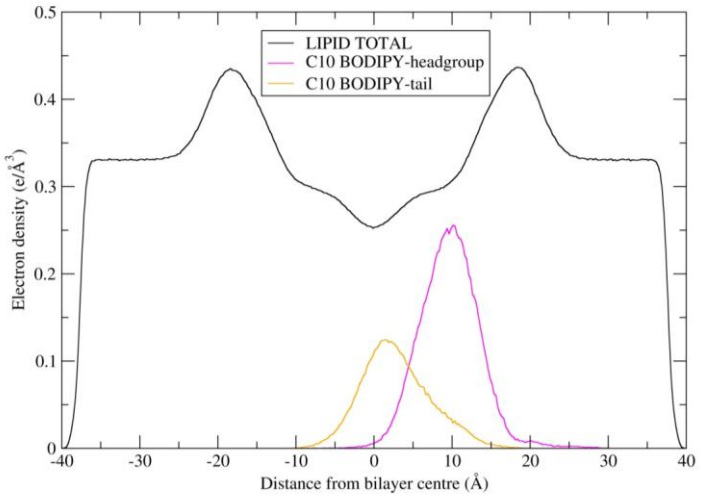

b)

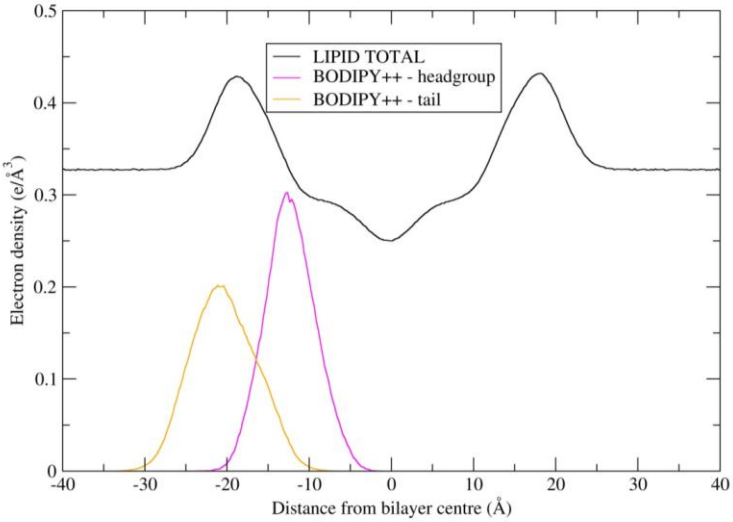

c)

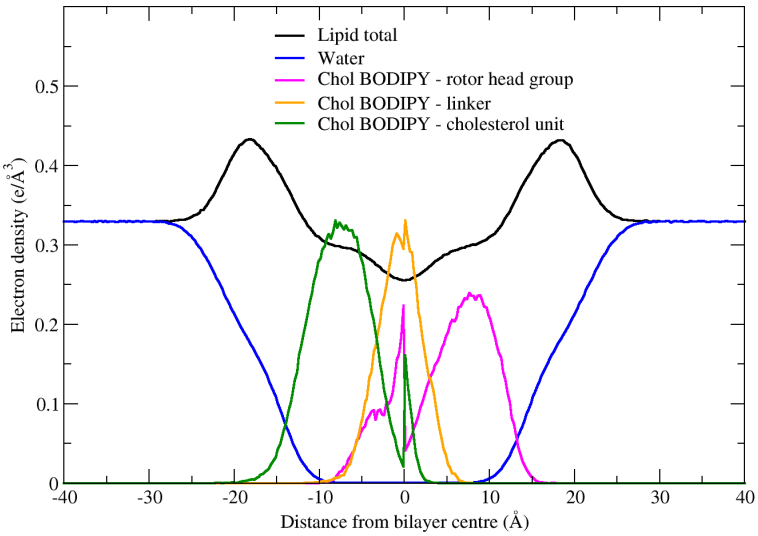

Fig. S2 Simulated electron density profiles for a) rotor **1**, b) rotor **2** and c) rotor **3** in DOPC bilayers. The BODIPY head group is in a similar position in the bilayer for all three rotors

(2) The BODIPY Molecular Rotors

Calibration data for rotors **1**[16] and **2**[17] in methanol:glycerol mixtures have been previously reported, and is shown in Fig S2. All three rotors display a linear correlation between log (viscosity) and log (fluorescence lifetime) within the range of ca. 10-1000 cP in agreement with the Förster-Hoffmann equation.

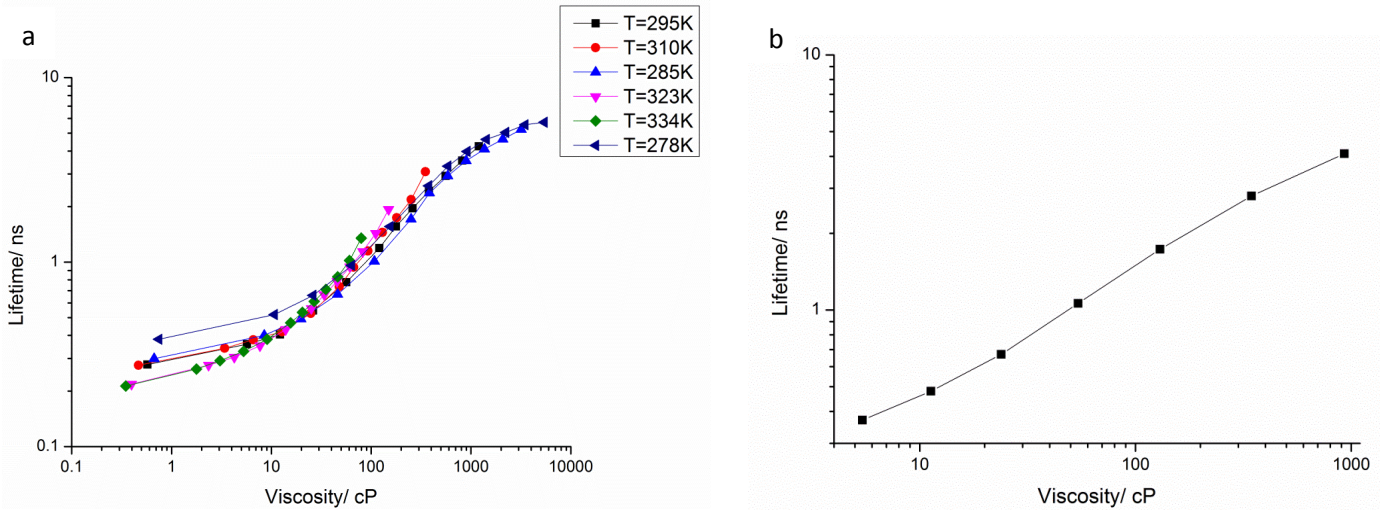

Fig. S3 Calibration plots for rotors **1** (a) and **2** (b) in methanol:glycerol mixtures

Overlaid absorption and emission spectra for the three rotors are shown in Fig. S3. The spectra are almost identical, suggesting that the electronic structures of the fluorophores are very similar.

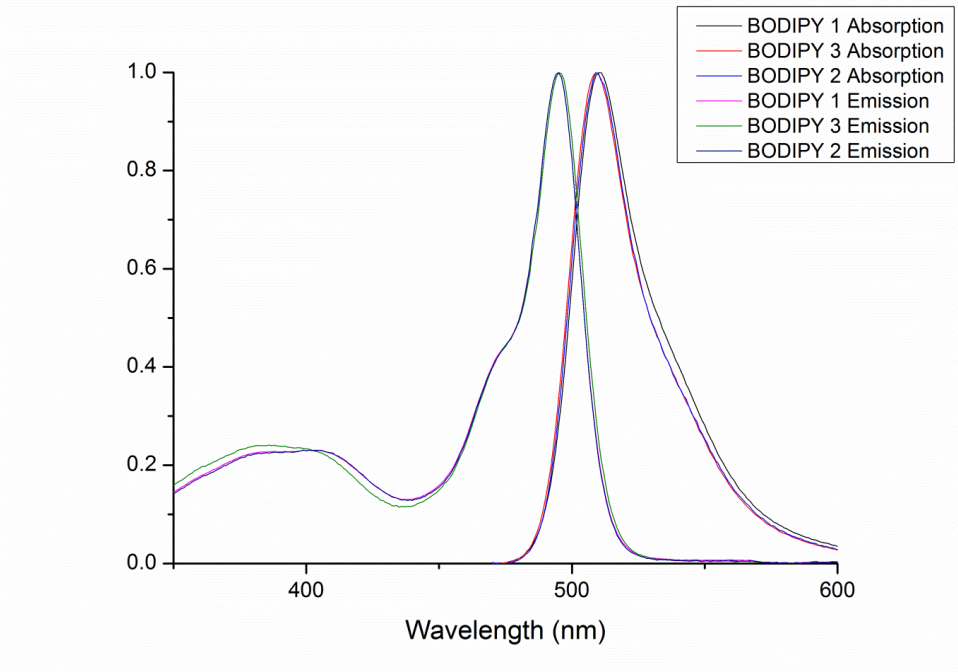

Fig. S4 Overlaid emission and absorption spectra of the three rotors (with the maximum for each spectrum normalised to 1)

At low viscosities, the lifetime of the BODIPY rotors is influenced by solvent polarity.

Fig. S5 shows fluorescence decays of Rotor **1** in a range of non-viscous solvents of varying polarity. There are significant differences in the decay traces.

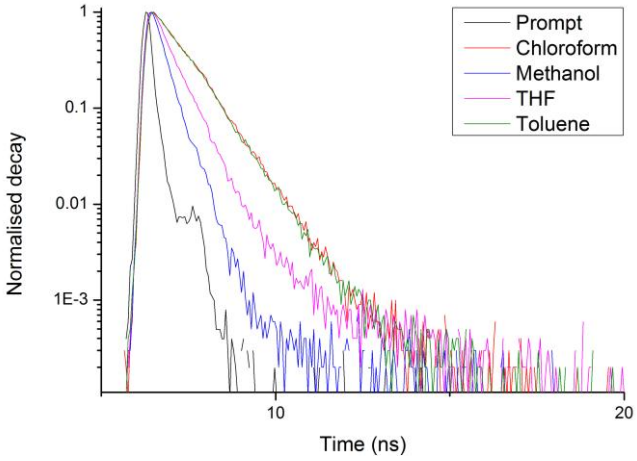

Fig. S5 Fluorescence decays of Rotor **1** in chloroform, methanol, THF and toluene, 4 solvents of similar viscosity and different polarity.

At higher viscosities, the influence of polarity on lifetime decreases. Fig. S6 shows fluorescence lifetimes of rotor **1** in three viscous diols between 10 and 100 cP at a range of temperatures. Each diol will have a different polarity, so the degree of overlap between the different lifetimes will show the influence of polarity on the lifetime of the rotor at increasing viscosity. As viscosity increases, the degree of overlap also increases, suggesting that polarity has a diminishing effect on the lifetime as the viscosity increases.

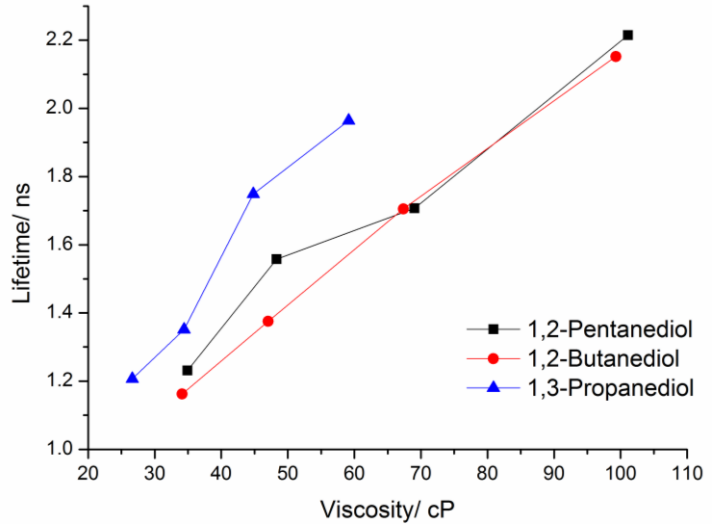

Fig. S6 Fluorescence lifetimes of rotor **1** in 1,2-pentanediol, 1,2-butanediol and 1,3-propanediol at 10, 15, 20 and 25 ^{o}C

In order to further investigate the effect of polarity on lifetime of BODIPY rotors, rotor **1** was dissolved in castor oil, a viscous non-polar solvent, and the change in lifetime with viscosity was compared with the methanol:glycerol calibration mixtures, i.e. much more polar environments. The fluorescence decays of rotor **1** in castor oil are shown in Fig. S7.

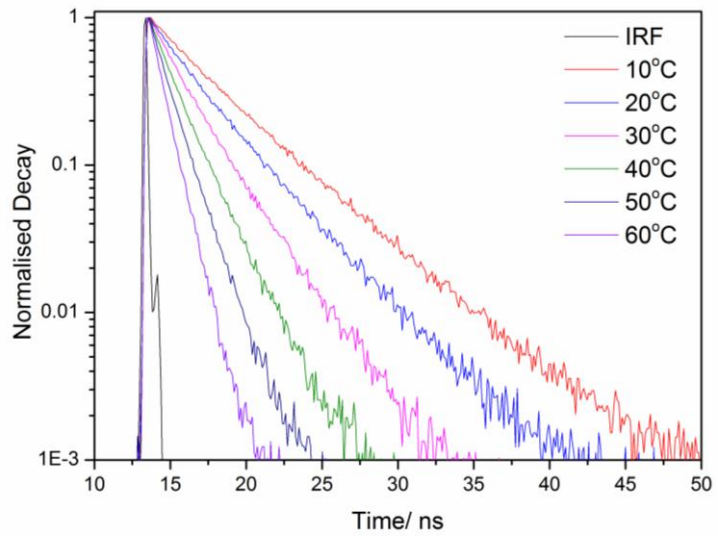

Fig. S7 Fluorescence decays of rotor **1** in castor oil

Castor oil is intrinsically fluorescent, resulting in biexponential decays. This autofluorescence is very weak, and contributed a small percentage (20 %) of the decay trace obtained for rotor **1** in castor oil at 25 ^{o}C, so the viscosity sensitive component of the biexponential decays was treated as the lifetime of rotor **1** without influence from the castor oil. Fig. S8 shows the fluorescence decay of pure castor oil at 25 °C.

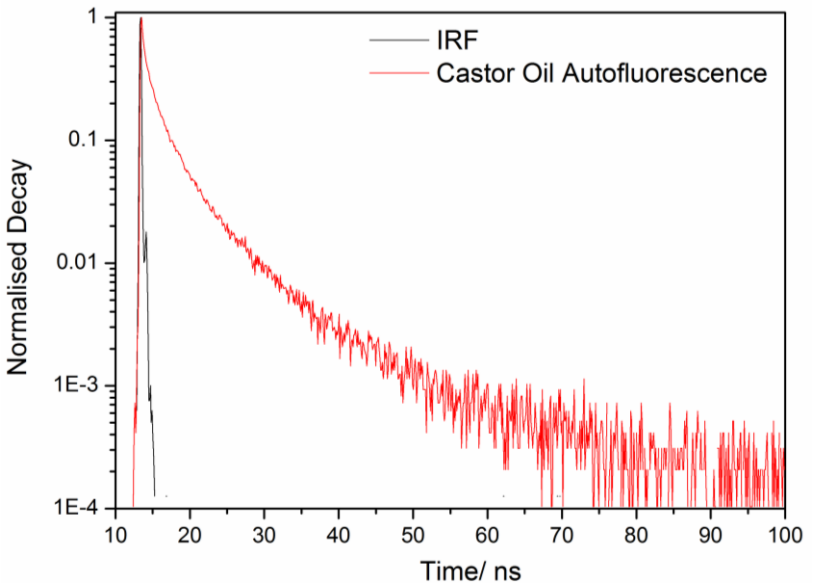

Fig. S8 Fluorescence decay of pure castor oil at 25 °C, highlighting the autofluorescence of castor oil. Acquisition time was approximately 100 times that of Fig S7 on the same collection settings

(3) BODIPY rotors in LUVs

Fig. S9 shows fluorescence decays of rotors **1** and **2** in DOPC and EYSM/DPPC. The short lifetime component seen in the decays rotor **2** is attributed to rotor dissolved in the aqueous phase, owing to its water solubility.

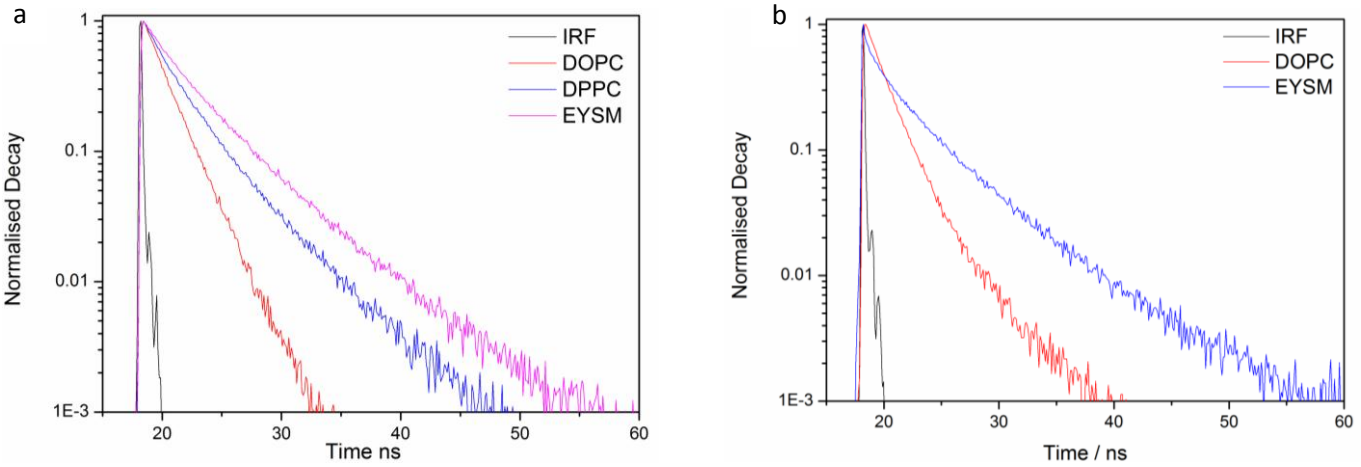

Fig. S9 fluorescence decays of rotor **1** (a) and rotor **2** (b) in DOPC and DPPC/EYSM. The short lifetime component observed for rotor **2** is attributed to it partitioning into the water phase and represents approximately 15 % of the signal..

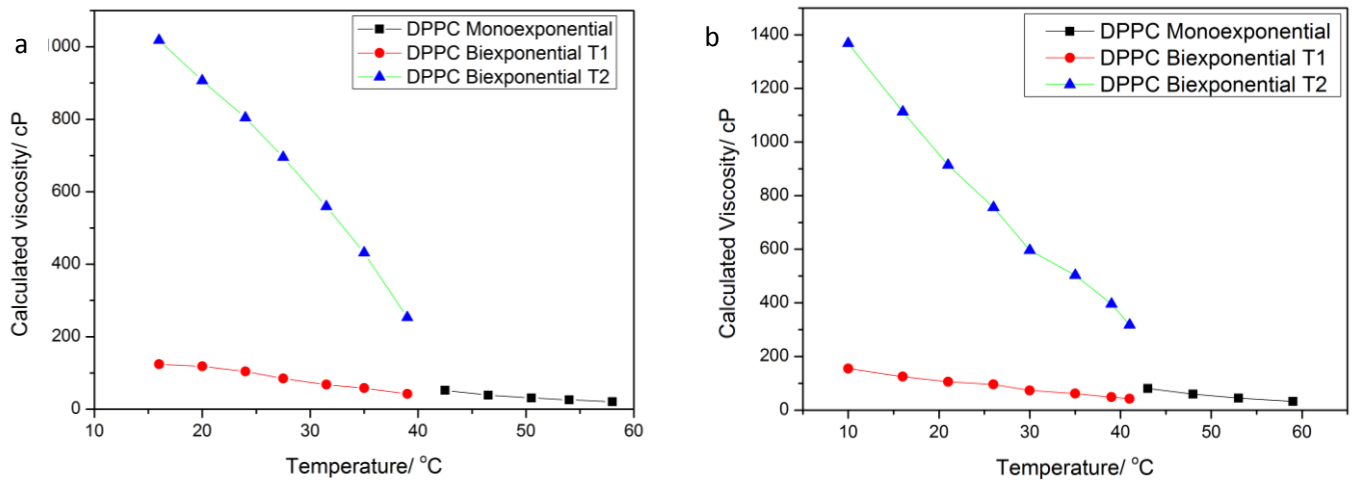

Fig. S10 Calculated viscosities for a) rotor **1** and b) rotor **2** in DPPC LUVs, highlighting the sensitivity to the phase transition within a DPPC bilayer. Note the viscosity values are identical to those measured by rotor **3** (Fig 4b)

(4) Parameters for Saffman-Delbrück Calculations

The Saffman-Delbrück formula is shown below:

$$D_{sd} = \frac{k_B T}{4\pi\eta_m h}\left[\ln\left(\frac{2L_{sd}}{a}\right) - \gamma\right]$$

Where D_{sd} is the Saffman-Delbrück diffusion coefficient, a is the radius of the membrane inclusion, h is the bilayer thickness, η_m is the membrane viscosity, γ is the Euler-Mascheroni constant (γ ≈ 0.577), and L_{sd} is the Saffman-Delbrück length, given by:

$$L_{sd} = \frac{h\eta_m}{2\eta_f}$$

Where η_f is the viscosity of the surrounding fluid. Table S2 shows the values for each parameter, with a reference given where necessary. Values for a were taken from the AMBER simulations.

Parameter	Value	Reference
η_m	From lifetime	n/a
η_f	0.8903 cP	18
a *(rotor **1**)*	6.20 Å	n/a
a *(rotor **2**)*	6.97 Å	n/a
a *(rotor **3**)*	8.28 Å	n/a
DOPC bilayer thickness	37 Å	5

Table S2 values of the parameters used in the Saffman-Delbrück calculations

(5) Studies in Phase-Separated GUVs

The phase diagram of DOPC:EYSM:Chol is shown in Fig. S9, highlighting the tie-lines through the L_o-L_d phase coexistence region and showing the compositions of GUVs **A**, **B**, **C** and **D**.

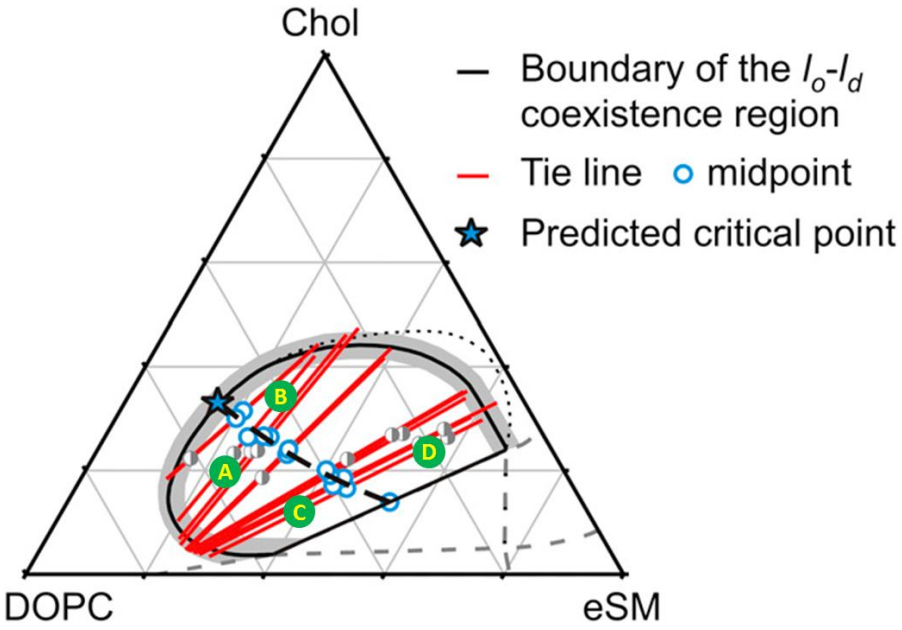

Fig. S11 Phase diagram of DOPC:EYSM:Chol, showing tie-lines and compositions of GUVs **A**, **B**, **C** and **D**.[19]

Histograms for the fluorescence lifetimes of the four individual GUVs stained with Rotor **1** shown in Fig. 7 are shown in Fig. S10. There are two peaks in each histogram, representing the L_o and L_d phases of each GUV. Note that due to the poor partitioning of the rotor into the L_o phase, there is less signal from the L_o phases in each of the histograms, resulting in lower intensities.

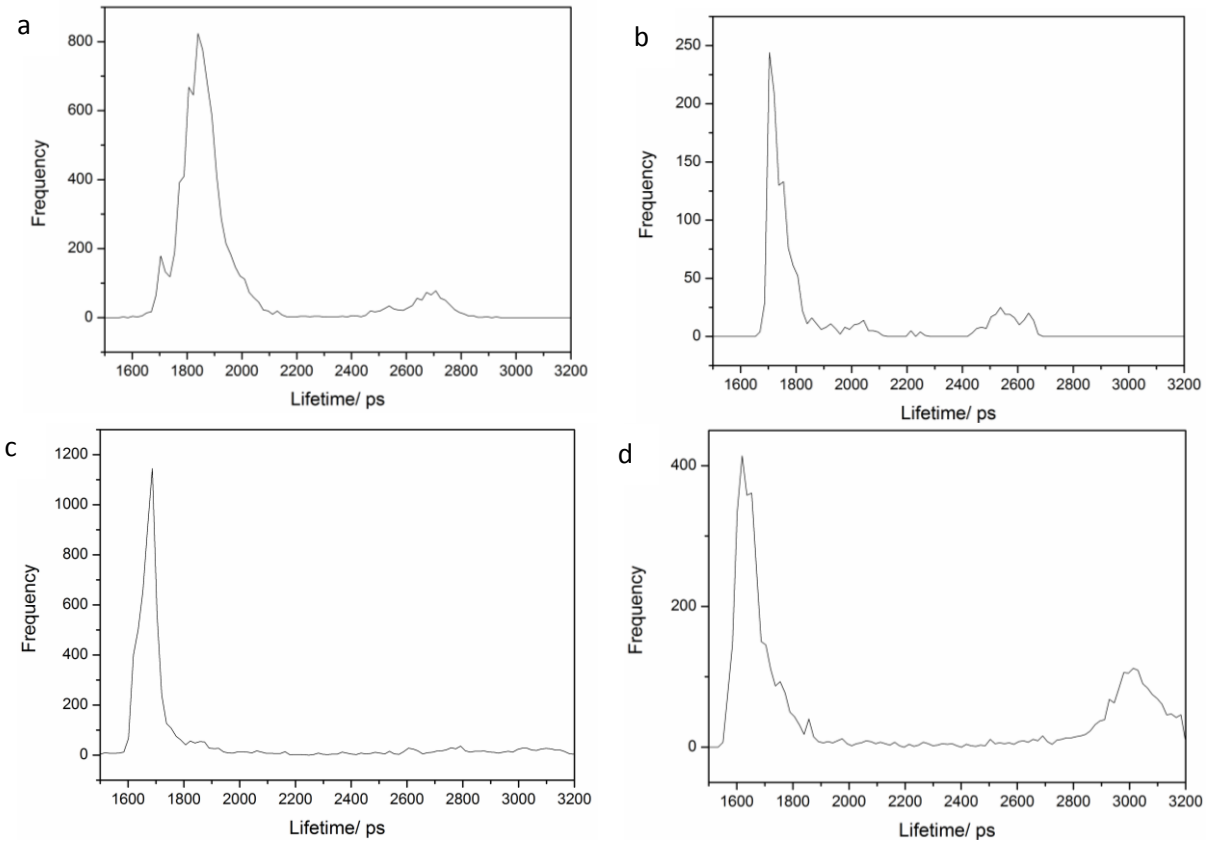

Fig. S12 Lifetime distribution histograms for the individual GUVs **A**, **B**, **C** and **D** shown in Fig. 7

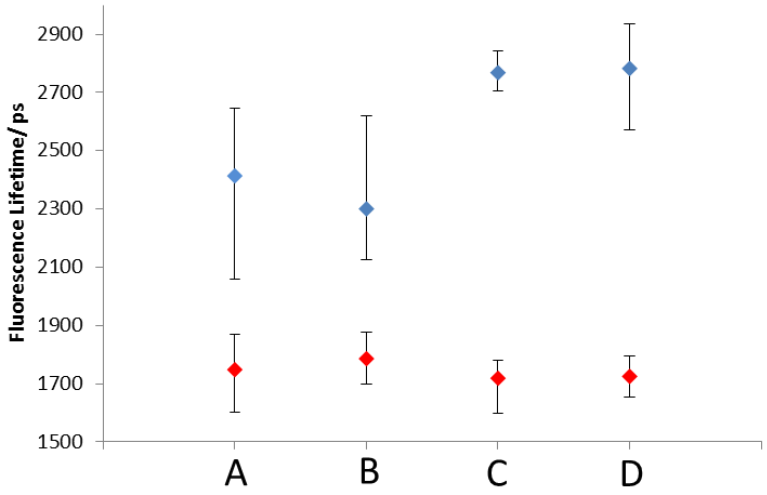

Fig. S13 Plot showing the average lifetimes and error bars for the viscosities shown in Table 2. L_d phases are shown in red and L_o phases in blue.

(6) Synthesis of Rotor 3

1.1 General Materials and Methods

The manipulation of all air and/or water sensitive compounds was carried out using standard inert atmosphere techniques. All chemicals were used as received from commercial sources without further purification. Anhydrous solvents were used as received from commercial sources. Analytical thin layer chromatography (TLC) was carried out on Merck® aluminium backed silica gel 60 GF254 plates and visualization when required was achieved using UV light or I_2. Flash column chromatography was performed on silica gel 60 GF254 using a positive pressure of nitrogen with the indicated solvent system. Where mixtures of solvents were used, ratios are reported by volume.

Nuclear magnetic resonance spectra were recorded on 400 MHz spectrometers at ambient probe temperature. Chemical shifts for ^{1}H NMR spectra are recorded in parts per million from tetramethylsilane with the solvent resonance as the internal standard (chloroform: δ = 7.27 ppm). ^{13}C NMR spectra were recorded with complete proton decoupling. Chemical shifts are reported in parts per million from tetramethylsilane with the solvent resonance as the internal standard ($^{13}CDCl_3$: 77.0 ppm). ^{19}F NMR spectra were recorded with complete proton decoupling. Chemical shifts are reported in parts per million referenced to the standard hexafluorobenzene: −164.9 ppm. Mass spectra were carried out using ElectroSpray Ionization (ESI), and only molecular ions are reported. Infrared spectra (ν_{max}, FTIR ATR) were recorded in reciprocal centimeters (cm^{-1}).

1.2 Synthetic Procedures

Compound 8. *tert*-Butyl(chloro)diphenylsilane (4.3 g, 15.6 mmol) was added to a mixture of lithocholic acid (2 g, 5.3 mmol) and imidazole (1.4 g, 20.5 mmol) in dry *N,N*-dimethylformamide (20 mL) at 0 °C. The reaction mixture was allowed to warm to room temperature and stirred overnight. Then, the reaction mixture was diluted with Et_2O (100 mL), washed with H_2O (3 x 100 mL) and dried over anhydrous $MgSO_4$. The solvent was evaporated under vacuum and the residue was purified by flash chromatography (1:2 CH_2Cl_2:petroleum ether), R_f 0.35, to give **8** as a colorless oil. Yield: 3.1 g (70%).

^{1}H NMR (400 MHz, $CDCl_3$) δ_H 7.71-7.69 (m, 8H), 7.45-7.36 (m, 12H), 3.64 (sept, *J* = 4.6 Hz, 1H), 2.53-2.49 (m, 1H), 2.44-2.37 (m, 1H), 1.97-1.13 (m, 25H), 1.13 (s, 9H), 1.07 (s, 9H), 0.97 (d, *J* = 6.2 Hz, 3H), 0.83 (s, 3H), 0.75 (td, *J* = 14, 3.5 Hz, 1H), 0.63 (s, 3H); **^{13}C NMR** (100 MHz, $CDCl_3$) δ_C 173.43, 135.78, 135.34, 135.02, 134.91, 132.08, 129.98, 129.38, 127.66, 127.43, 127.41, 73.58, 56.37, 56.10, 42.76,

42.11, 40.35, 40.14, 36.63, 35.84, 35.41, 35.30, 34.48, 33.19, 31.24, 30.81, 28.22, 27.21, 27.05, 26.95, 26.39, 24.20, 23.30, 20.83, 19.15, 18.30, 12.04; **MS (ESI)** m/z 875.5189 ($C_{56}H_{76}O_3Si_2$, $[M+Na]^+$, requires 875.5231); **IR (neat)** 2930, 2859, 1726, 1590, 1471, 1427, 1371, 1248, 1167, 1106, 933 cm^{-1}.

Compound 7. $LiAlH_4$ (2 mL, 1M in THF) was added dropwise to a solution of compound **8** (1.6 g, 1.8 mmol) in dry THF (10 mL) under nitrogen atmosphere at 0 °C. After the addition, the reaction mixture was allowed to warm at room temperature and stirred overnight. The reaction mixture was cooled at 0 °C and a saturated solution of $NaHCO_3$ was added carefully, and the resulting mixture was extracted with $CHCl_3$ (3 x 50 mL). The organic solution was dried over anhydrous $MgSO_4$, filtered and evaporated under vacuum. The residue was purified by flash chromatography (2:1 CH_2Cl_2:petroleum ether), R_f 0.38, to give compound **5** as a colorless oil. Yield: 1.2 g (92%).

^{1}H NMR (400 MHz, $CDCl_3$) δ_H 7.70-7.68 (m, 4H), 7.43-7.35 (m, 6H), 3.63 (m, 3H), 1.97-1.13 (m, 27H), 1.06 (s, 9H), 0.95 (d, *J* = 6.2 Hz, 3H), 0.82 (s, 3H), 0.74 (td, *J* = 14, 3.5 Hz), 0.62 (s, 3H); **^{13}C NMR** (100 MHz, $CDCl_3$) δ_C 135.79, 135.03, 134.92, 129.38, 127.42, 127.41, 73.61, 63.63, 56.40, 56.24, 42.72, 42.12, 40.36, 40.15, 36.63, 35.85, 35.58, 35.41, 34.48, 31.87, 30.81, 29.45, 28.33, 27.23, 27.05, 26.41, 24.21, 23.31, 20.83, 19.15, 18.67, 12.03; **MS (ESI)** m/z 601.4443 ($C_{40}H_{61}O_2Si$, $[M+H]^+$, requires 601.4441); **IR (neat)** 3330, 2929, 2859, 1590, 1464, 1447, 1427, 1371, 1106, 1072, 1012, 949 cm^{-1}.

Compound 6. Methanesulfonyl chloride (0.3 mL, 3.8 mmol) was added to a mixture of Et_3N (0.8 mL, 5.8 mmol) and **7** (1.1 g, 1.8 mmol) in dry CH_2Cl_2 (10 mL) at 0 °C. The reaction mixture was allowed to warm to room temperature and stirred for 5 h. Then, the reaction mixture was diluted with CH_2Cl_2 (100 mL), washed with H_2O (3 x 100 mL) and dried over anhydrous $MgSO_4$. The solvent was removed and the residue was purified by flash chromatography (1:1 CH_2Cl_2:petroleum ether), R_f 0.37, to give compound **6** as a colorless oil. Yield: 1.1 g (90%).

^{1}H NMR (400 MHz, $CDCl_3$) δ_H 7.69-7.68 (m, 4H), 7.43-7.35 (m, 6H), 4.24-4.18 (td, *J* = 6.5, 2.5 Hz, 2H), 3.64 (sept, *J* = 4.6 Hz, 1H), 3.02 (s, 3H), 1.97-1.13 (m, 27H), 1.06 (s, 9H), 0.95 (d, *J* = 6.2 Hz, 3H), 0.82 (s, 3H), 0.74 (td, *J* = 14, 3.5 Hz, 1H), 0.63 (s, 3H); **^{13}C NMR** (100 MHz, $CDCl_3$) δ_C 135.78, 135.01, 134.91, 129.38, 127.43, 127.42, 73.59, 70.66, 56.37, 56.06, 42.74, 42.10, 40.33, 40.12, 37.42, 36.63, 35.84, 35.40, 35.32, 34.48, 31.55, 30.81, 28.30, 27.21, 27.05, 26.39, 25.89, 24.18, 23.30, 20.82, 19.15, 18.54, 12.02; **MS (ESI)** m/z 679.4207 ($C_{41}H_{63}O_4SiS$, $[M+H]^+$, requires 679.4216); **IR (neat)** 2935, 2857, 1590, 1471, 1428, 1351, 1171, 1105, 1091, 1056, 971, 916 cm^{-1}.

Compound 5. A mixture of **6** (1 g, 1.4 mmol), 4-hydroxybenzaldehyde (512 mg, 4.2 mmol) and potassium carbonate (580 mg, 4.2 mmol) in dry N,N-dimethylformamide (25 mL) was stirred at 80°C for 5 h, then cooled and diluted with Et_2O (200 mL). The organic solution was washed with H_2O (3 x

100 mL), dried over anhydrous $MgSO_4$, filtered and the solvents were removed by rotary evaporation. The crude product was purified by flash chromatography (2:1 CH_2Cl_2:petroleum ether), R_f 0.67, to give compound **5** as a colorless oil. Yield: 850 mg (86%).

^{1}H NMR (400 MHz, $CDCl_3$) δ_H 9.90 (s, 1H), 7.85 (d, *J* = 8.7 Hz, 2H), 7.71-7.69 (m, 4H), 7.43-7.36 (m, 6H), 7.02 (d, *J* = 8.7 Hz, 2H), 4.04 (td, *J* = 6.5, 2.5 Hz, 2H) 3.64 (sept, *J* = 4.6 Hz, 1H), 1.98-1.09 (m, 27H), 1.08 (s, 9H), 1.00 (d, J = 6.2 Hz, 3H), 0.83 (s, 3H), 0.78 (td, J = 14, 3.5 Hz, 1H), 0.66 (s, 3H); **^{13}C NMR** (100 MHz, $CDCl_3$) δ_C 190.72, 164.25, 135.75, 134.98, 134.87, 131.95, 129.75, 129.37, 127.41, 127.40, 114.75, 73.57, 68.91, 56.38, 56.13, 42.71, 42.08, 40.33, 40.12, 36.61, 35.82, 35.49, 35.39, 34.46, 32.03, 30.79, 28.30, 27.19, 26.39, 25.69, 24.19, 23.29, 20.81, 19.12, 18.63, 12.03; **MS (ESI)** m/z 705.4717 ($C_{47}H_{64}O_3Si$, $[M+H]^+$, requires 705.4703); **IR (neat)** 2929, 2858, 1691, 1599, 1577, 1471, 1427, 1371, 1311, 1253, 1214, 1157, 1107, 1073, 1007, 931 cm^{-1}.

Compound 4. To a solution of **5** (800 mg, 1.13 mmol) in THF (2 mL) was added a 1.0 M solution of tetrabutylammonium fluoride (TBAF) in THF (11 mL, 11 mmol), and the mixture was heated for 12 h at 40°C. The reaction was then quenched by addition of saturated aqueous NH_4Cl, and the mixture was extracted with $CHCl_3$ (3 x 100 mL). The combined organic extract was dried over anhydrous $MgSO_4$ filtered and the solvent was removed by rotary evaporation. The crude product was purified by flash chromatography ($CHCl_3$), R_f 0.1 , to afford compound **4** as a white solid. Yield: 365 mg (69%).

^{1}H NMR (400 MHz, $CDCl_3$) δ_H 9.88 (s, 1H), 7.84 (d, *J* = 8.7 Hz, 2H), 7.00 (d, *J* = 8.7 Hz, 2H), 4.02 (td, *J* = 6.5, 2.5 Hz, 2H), 3.64 (sept, *J* = 4.6 Hz, 1H), 2.00-1.09 (m, 28H), 0.97 (d, *J* = 6.2 Hz, 3H), 0.92 (s, 3H), 0.66 (s, 3H); **^{13}C NMR** (100 MHz, $CDCl_3$) δ_C 190.77, 164.26, 131.97, 129.76, 114.76, 71.84, 68.92, 56.52, 56.11, 42.72, 42.10, 40.45, 40.20, 36.46, 35.86, 35.51, 35.35, 34.57, 32.00, 30.55, 28.28, 27.19, 26.42, 25.69, 24.21, 23.36, 20.82, 18.60, 12.05; **MS (ESI)** m/z 467.3524 ($C_{31}H_{46}O_3$, $[M+H]^+$, requires 467.3525); **IR (neat)** 3582, 3491, 2929, 2861, 1675, 1601, 1574, 1510, 1446, 1426, 1383, 1302, 1252, 1219, 1158, 1112, 1089, 1009, 993, 945 cm^{-1}.

Rotor 3. A solution of **4** (640 mg, 1.36 mmol) in freshly distilled pyrrole (30 mL, 432 mmol) was degassed by bubbling with N_2 for 20 minutes before the addition of TFA (0.1 mL, 1.1 mmol). The mixture was stirred for 1 h at room temperature, diluted with $CHCl_3$ (100 mL) and then washed consecutively with H_2O (100 mL), $NaHCO_3$ (100 mL, 0.5M) and H_2O (100 mL). The organic extracts were dried over anhydrous $MgSO_4$, filtered and evaporated. The excess pyrrole was removed using high vaccum to give the corresponding dipyrromethane as a dark viscous oil. The crude dipyrromethane was purified by flash chromatography ($CHCl_3$) to give a green viscous oil. Yield: 745 mg (94%). The dipyrromethane (745 mg, 1.28 mmol) was dissolved in CH_2Cl_2 (25 mL) and DDQ (320 mg, 1.4 mmol) was added. The reaction mixture was stirred at room temperature shielded from light

for 1h. Then, Et_3N (2 mL, 14.3 mmol) was added, followed immediately by the addition of $BF_3{\cdot}(OEt_2)_2$ (1.5 mL, 12.1 mmol) and the reaction mixture was stirred at room temperature overnight. The organic solution was washed with H_2O (100 mL), NH_4Cl (100 mL, 0.5 M), $NaHCO_3$ (100 mL, 0.5 M) and finally H_2O (100 mL), then dried over anhydrous $MgSO_4$, filtered and evaporated to give a black viscous oil which was purified by column chromatography (3:1 petroleum ether:ethyl acetate), R_f 0.16, to afford rotor **3** as a red-orange solid. Yield: 240 mg (28%).

^{1}H NMR (400 MHz, $CDCl_3$) δ_H 7.91 (s, 1H), 7.54 (d, *J* = 8.8 Hz, 2H), 7.04 (d, *J* = 8.8 Hz, 2H), 6.98 (d, *J* = 3.9 Hz, 2H), 6.55 (d, *J* = 2.9 Hz, 2H), 4.02 (m, 2H), 3.63 (sept, *J* = 4.6 Hz, 1H), 2.00-1.09 (m, 28H), 0.99 (d, J = 6.2 Hz, 3H), 0.93 (s, 3H), 0.67 (s, 3H); **^{13}C NMR** (100 MHz, $CDCl_3$) δ_C 161.73, 147.52, 143.24, 134.77, 132.41, 131.31, 126.02, 118.18, 114.51, 71.79, 68.83, 56.50, 56.10, 42.70, 42.05, 40.41, 40.17, 36.39, 35.82, 35.52, 35.31, 34.54, 32.04, 30.49, 28.28, 27.16, 26.40, 25.76, 24.20, 23.34, 20.80, 18.60, 12.05; **^{19}F NMR** (377.5 MHz, $CDCl_3$) δ_F –148.23; **MS (ESI)** m/z 609.4035 ($C_{39}H_{51}BN_2O_2F_2$, $[M\text{-}F^-]^+$, requires 609.4028); **IR (neat)** 3582, 3361, 2925, 2861, 1602, 1573, 1508, 1411, 1426, 1383, 1295, 1252, 1223, 1158, 1176, 1113, 1073, 1043, 1011, 980, 911 cm^{-1}.

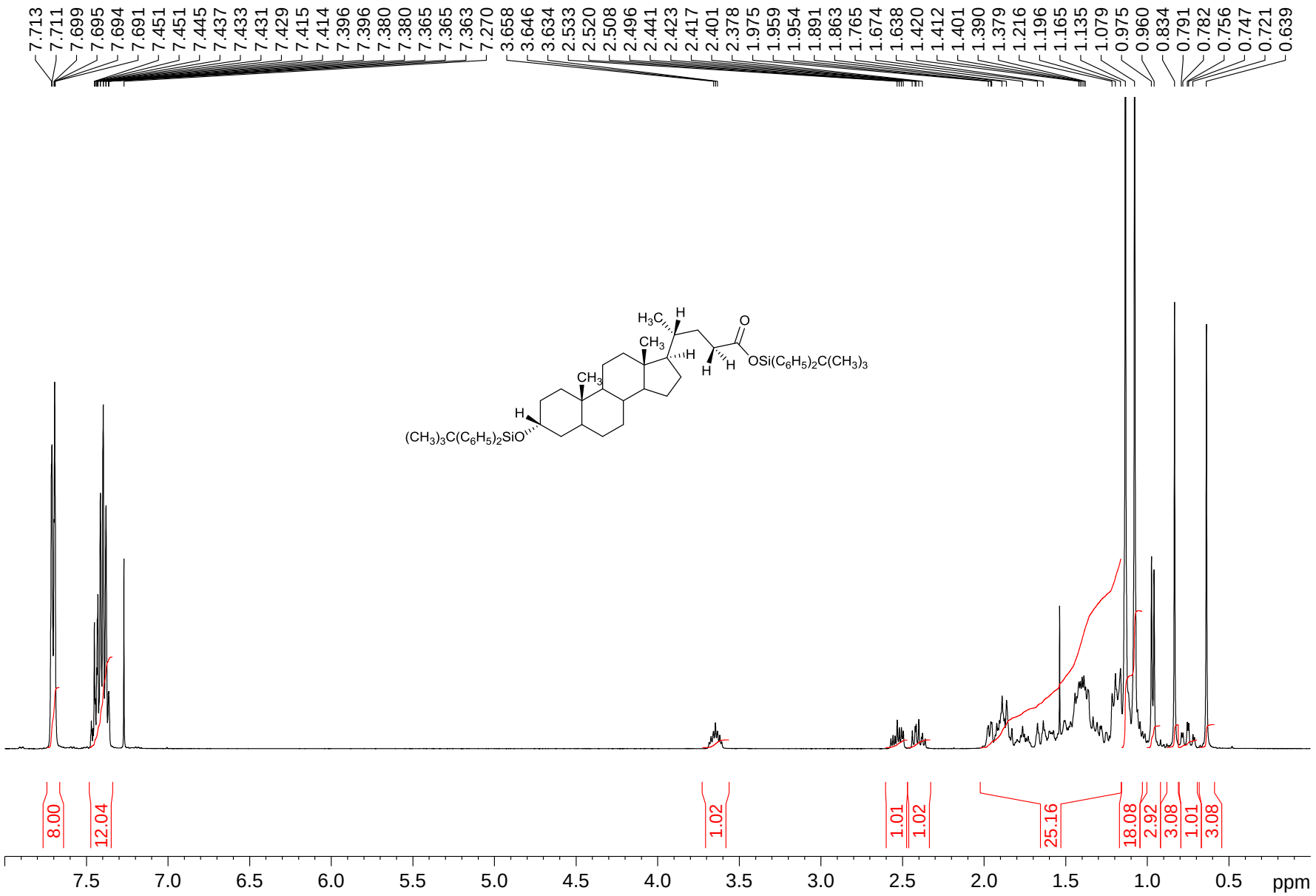

Fig. S14 ^{1}H NMR spectrum of **8** (400 MHz, $CDCl_3$).

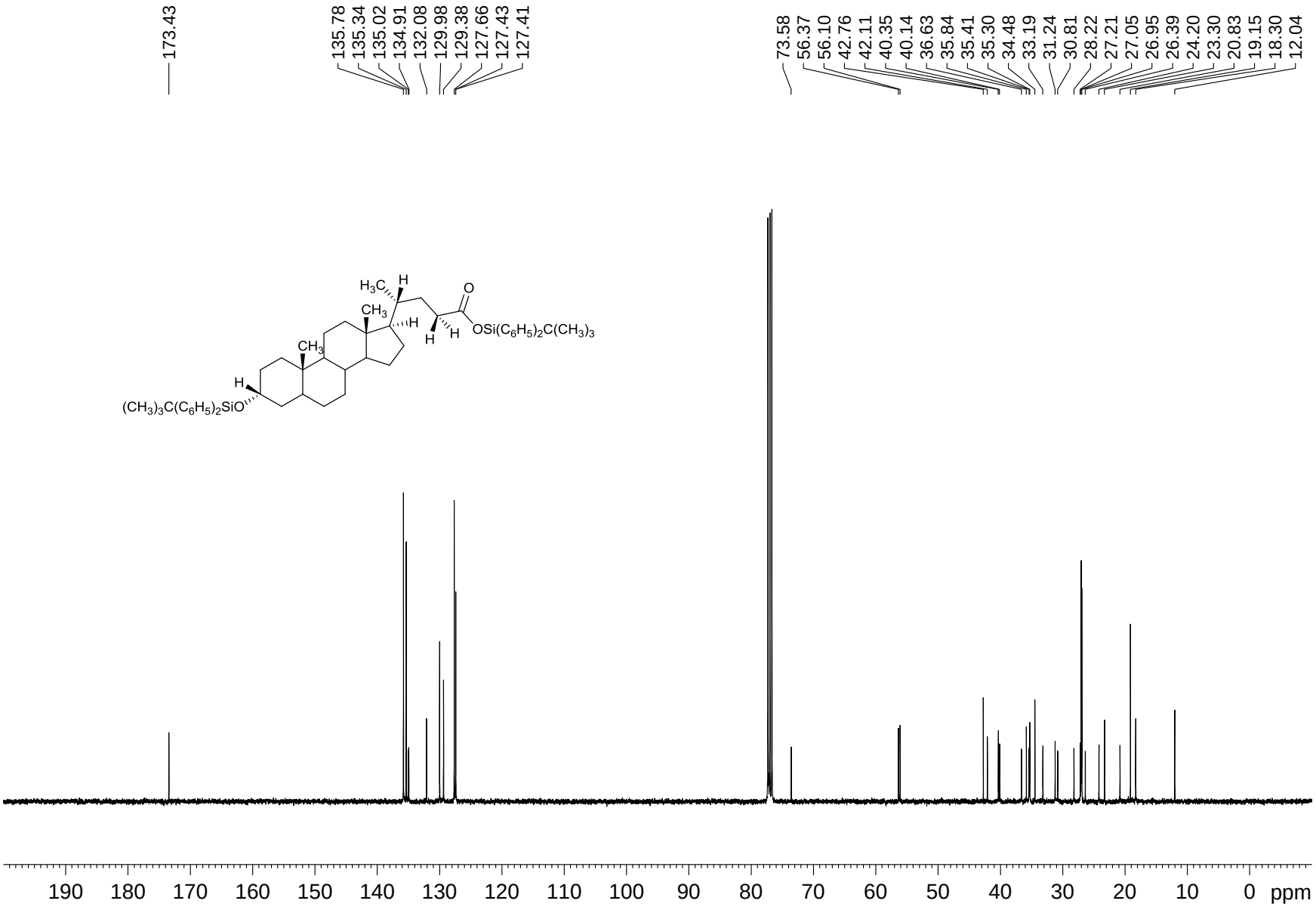

Fig. S15. ^{13}C NMR spectrum of **8** (100 MHz, $CDCl_3$).

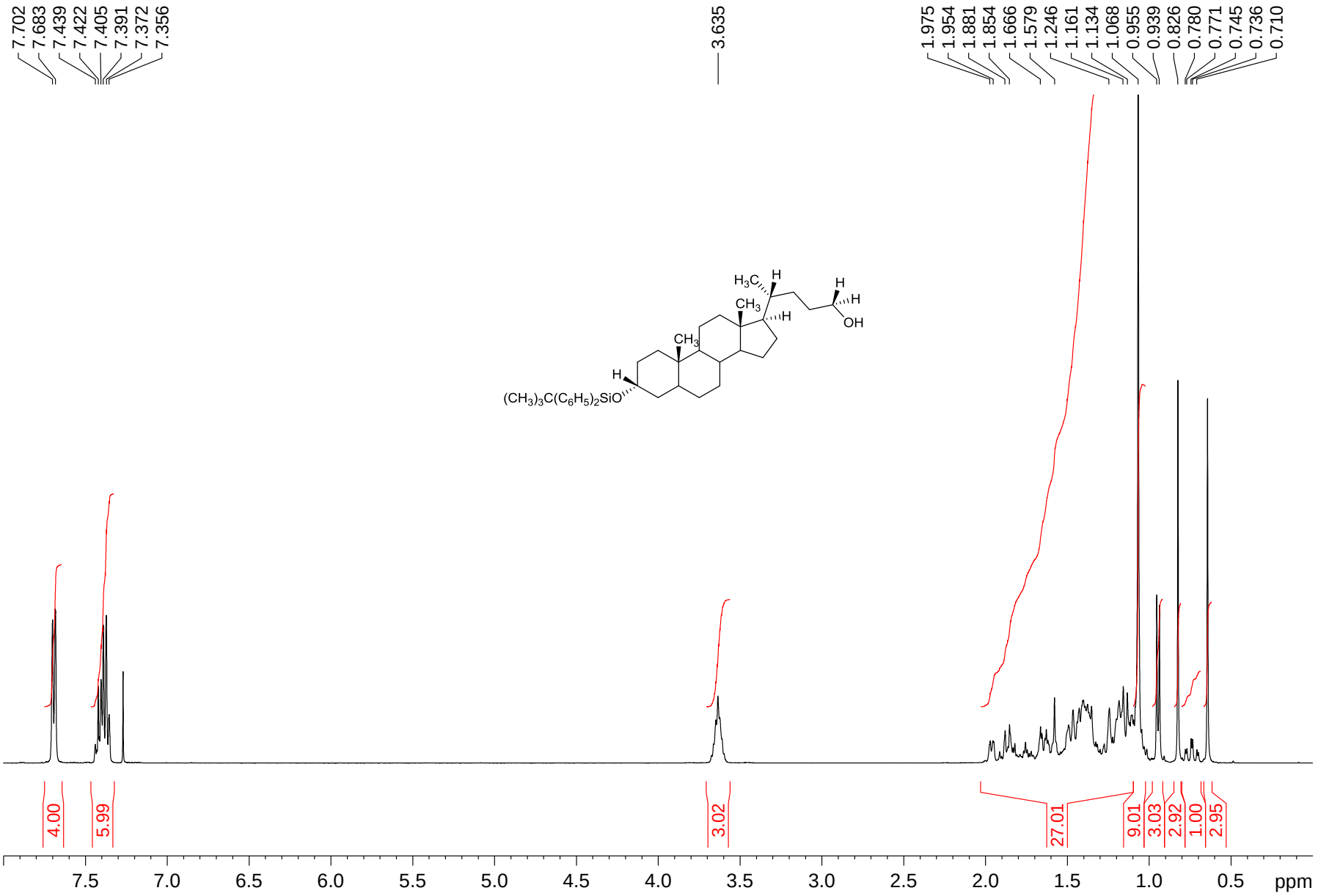

Fig. S16. ^{1}H NMR spectrum of **7** (400 MHz, $CDCl_3$).

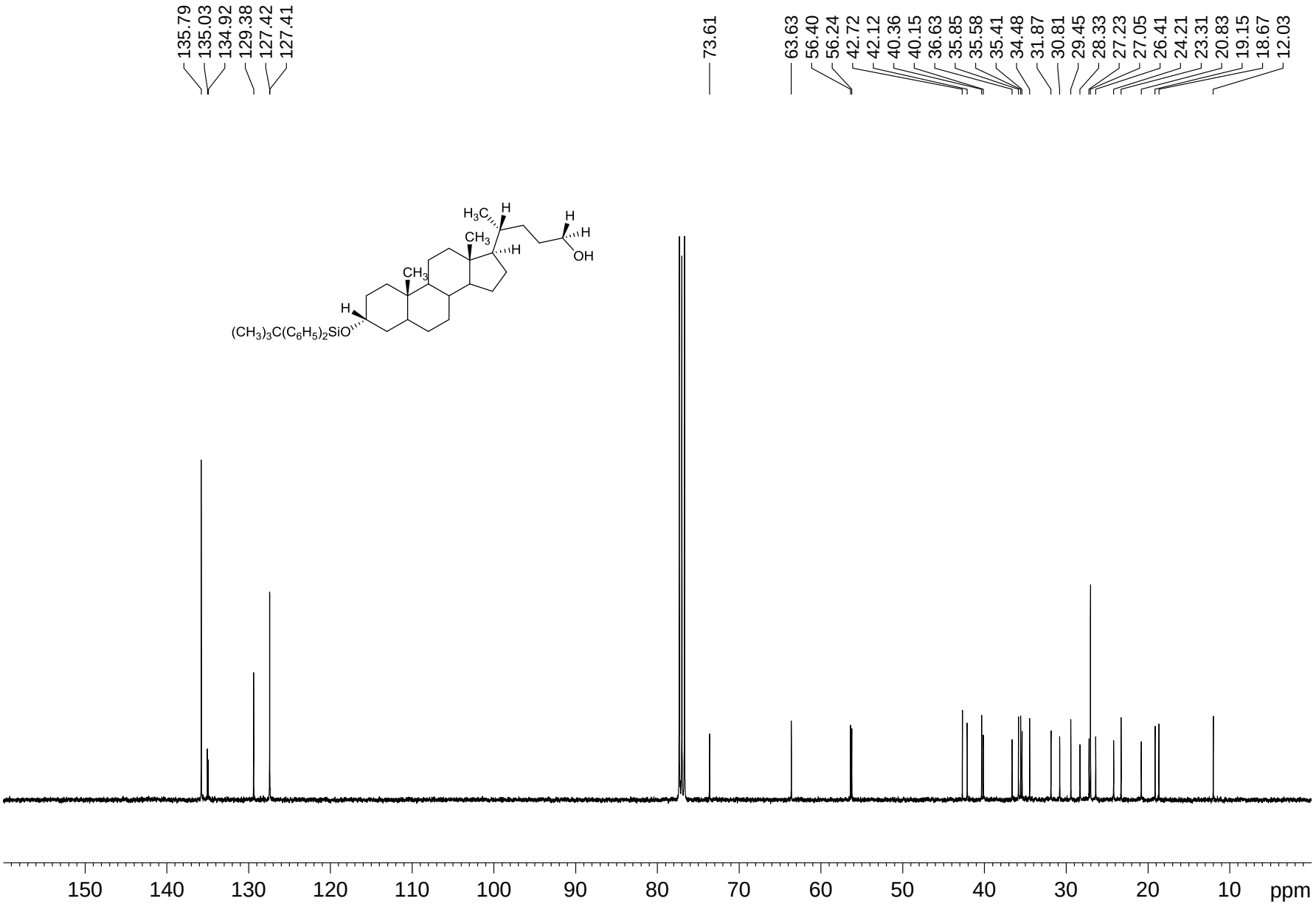

Fig. S17. ^{13}C NMR spectrum of **7** (100 MHz, $CDCl_3$).

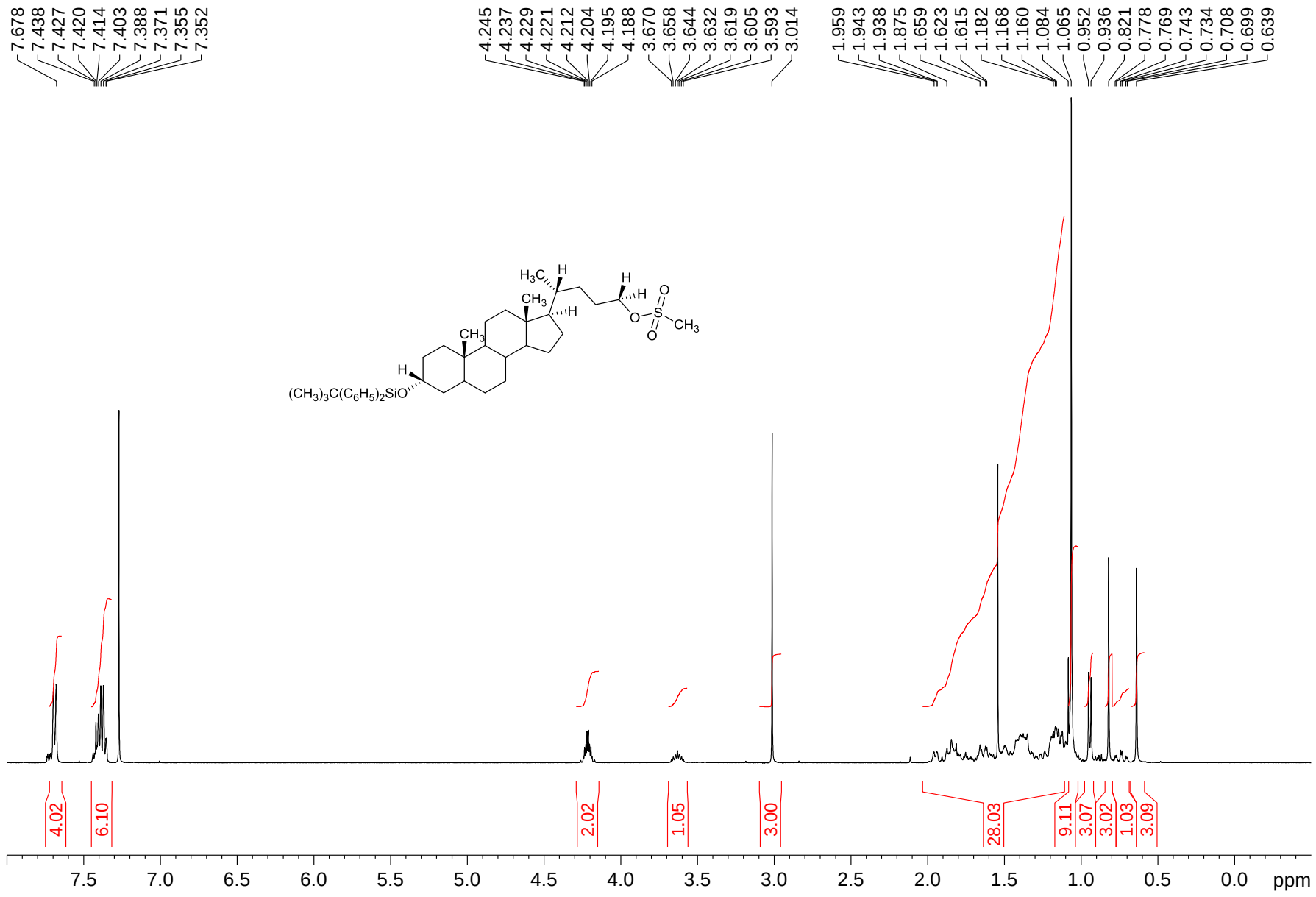

Fig. S18. ^{1}H NMR spectrum of **6** (400 MHz, $CDCl_3$).

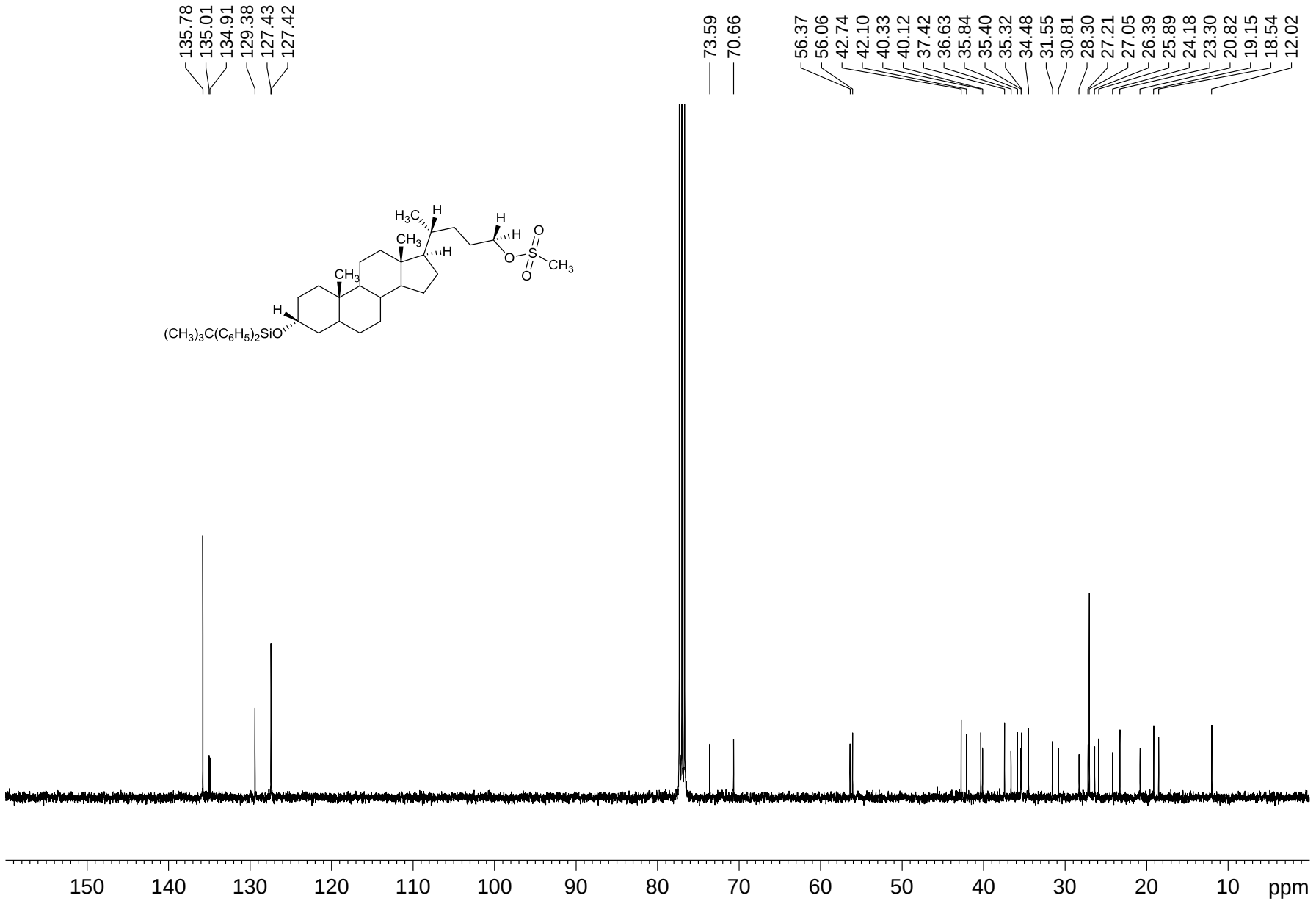

Fig. S19. ^{13}C NMR spectrum of **6** (100 MHz, $CDCl_3$).

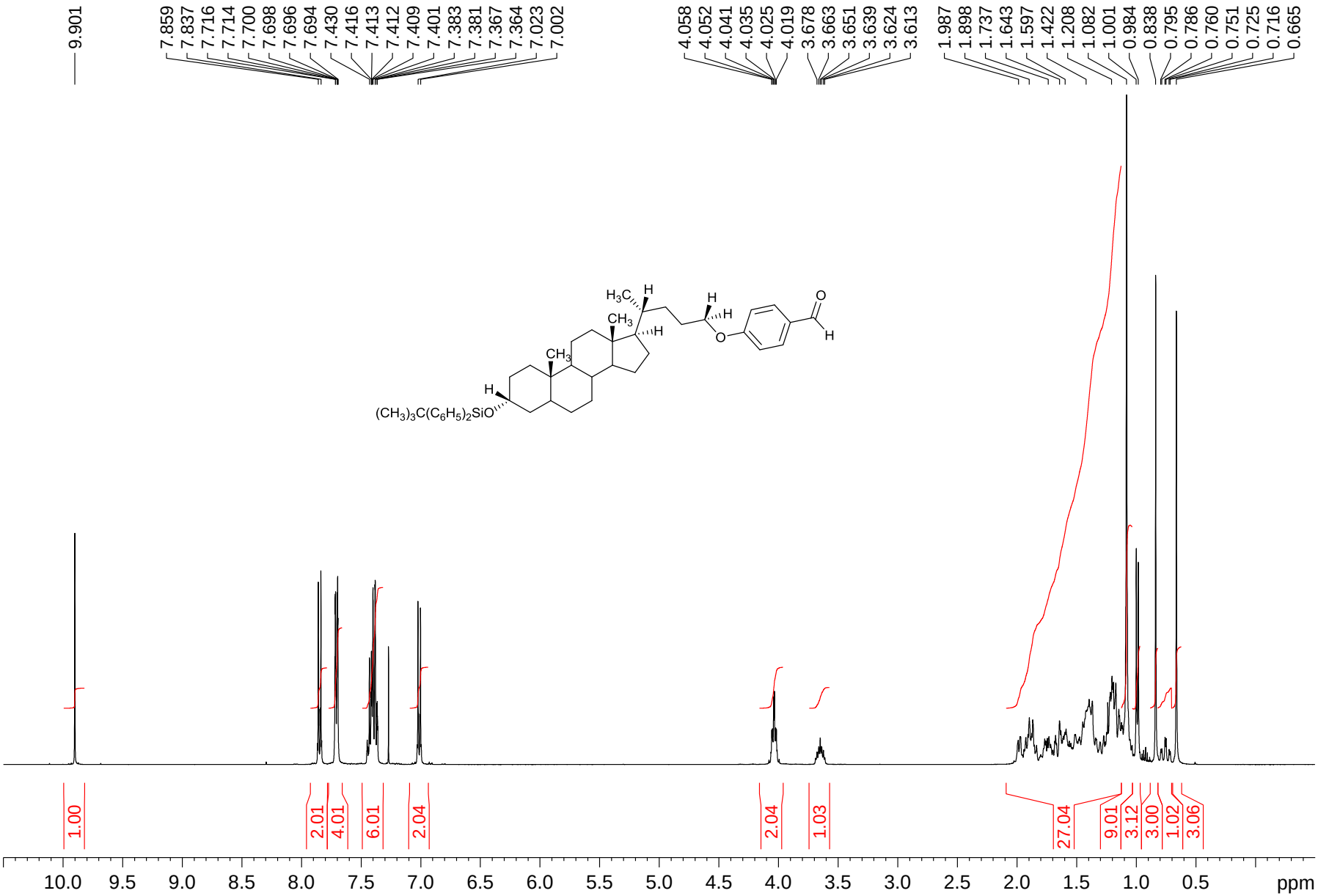

Fig. S20. ^{1}H NMR spectrum of **5** (400 MHz, $CDCl_3$).

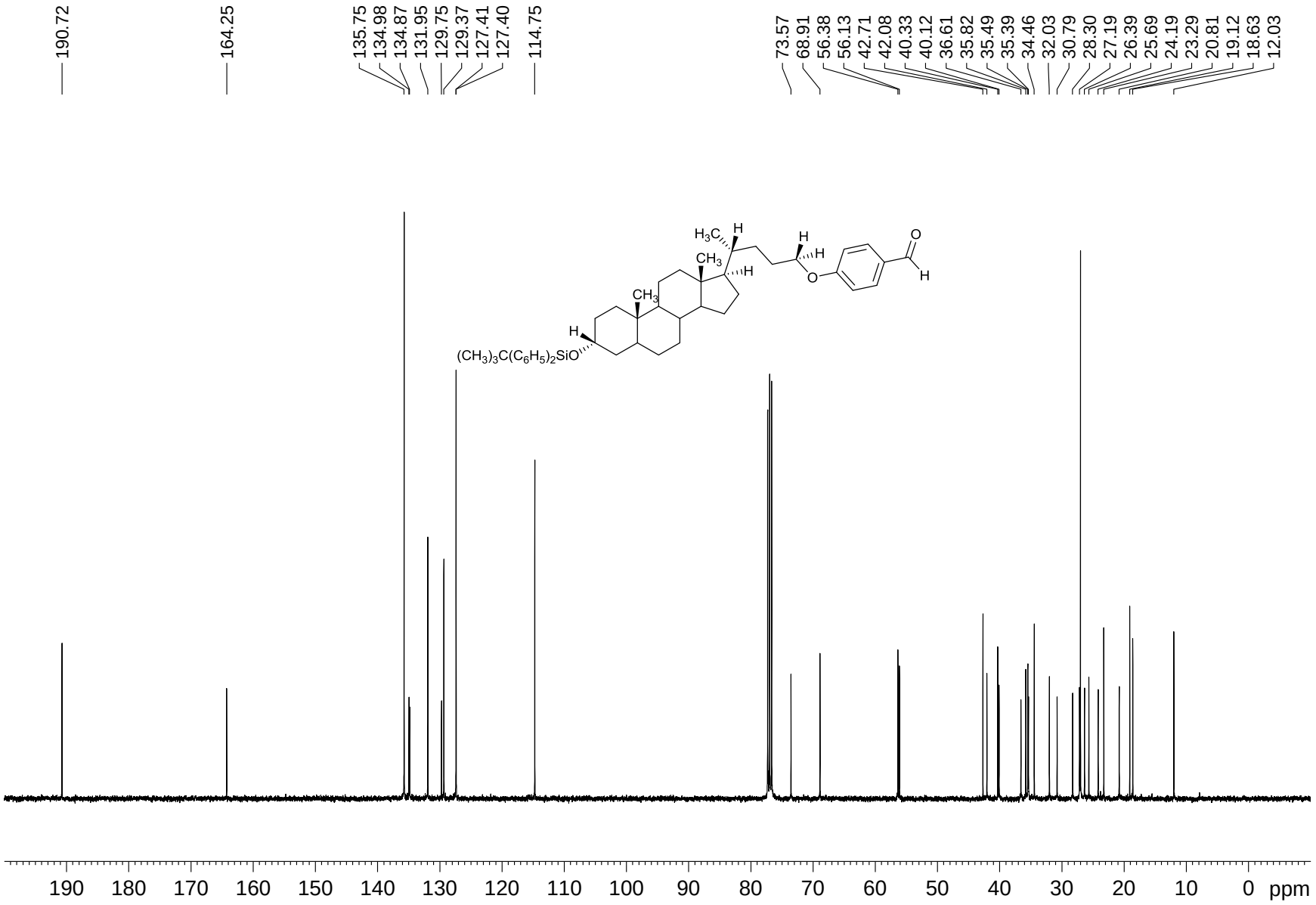

Fig. S21. ^{13}C NMR spectrum of **5** (100 MHz, $CDCl_3$).

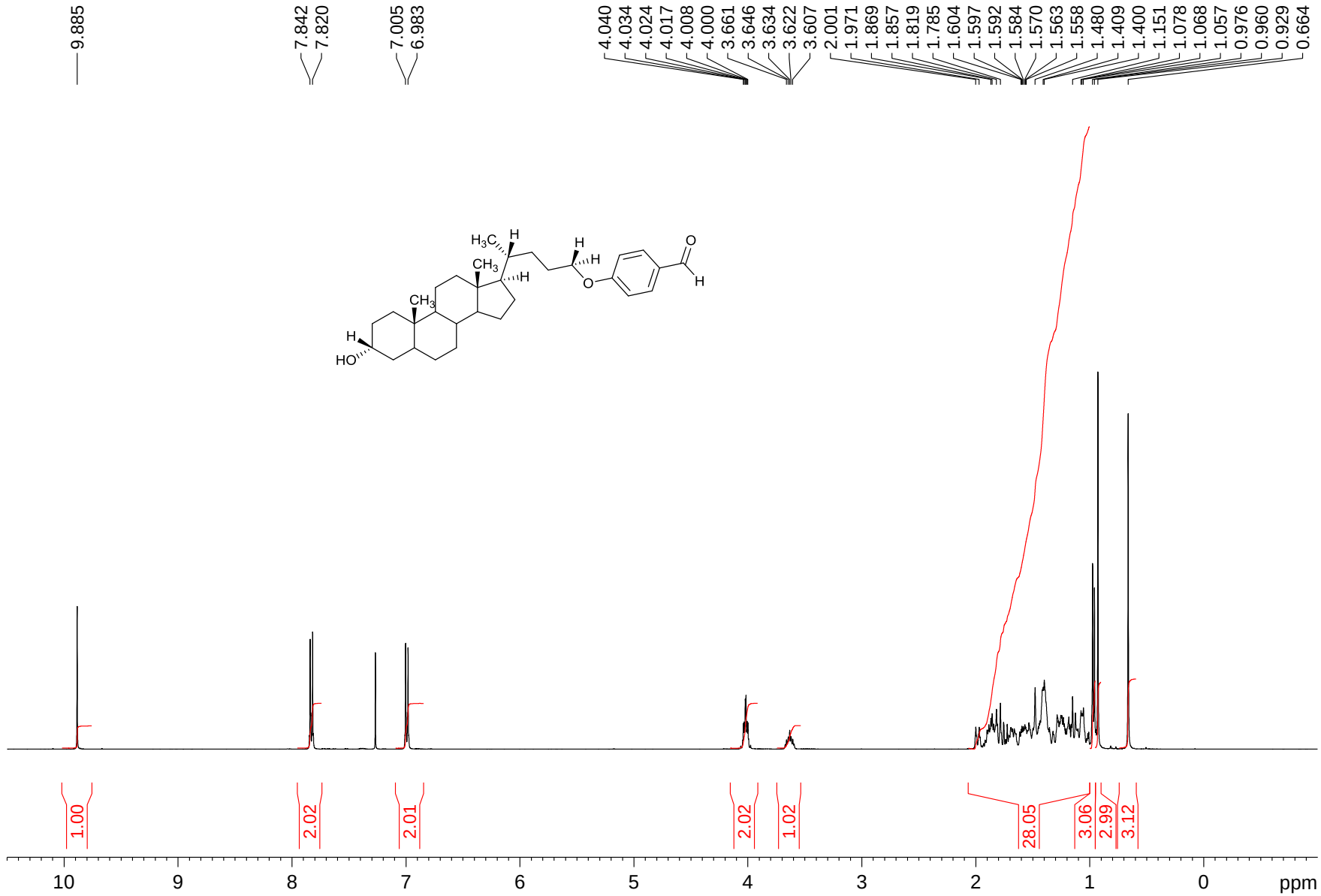

Fig. S22. ^{1}H NMR spectrum of **4** (400 MHz, $CDCl_3$).

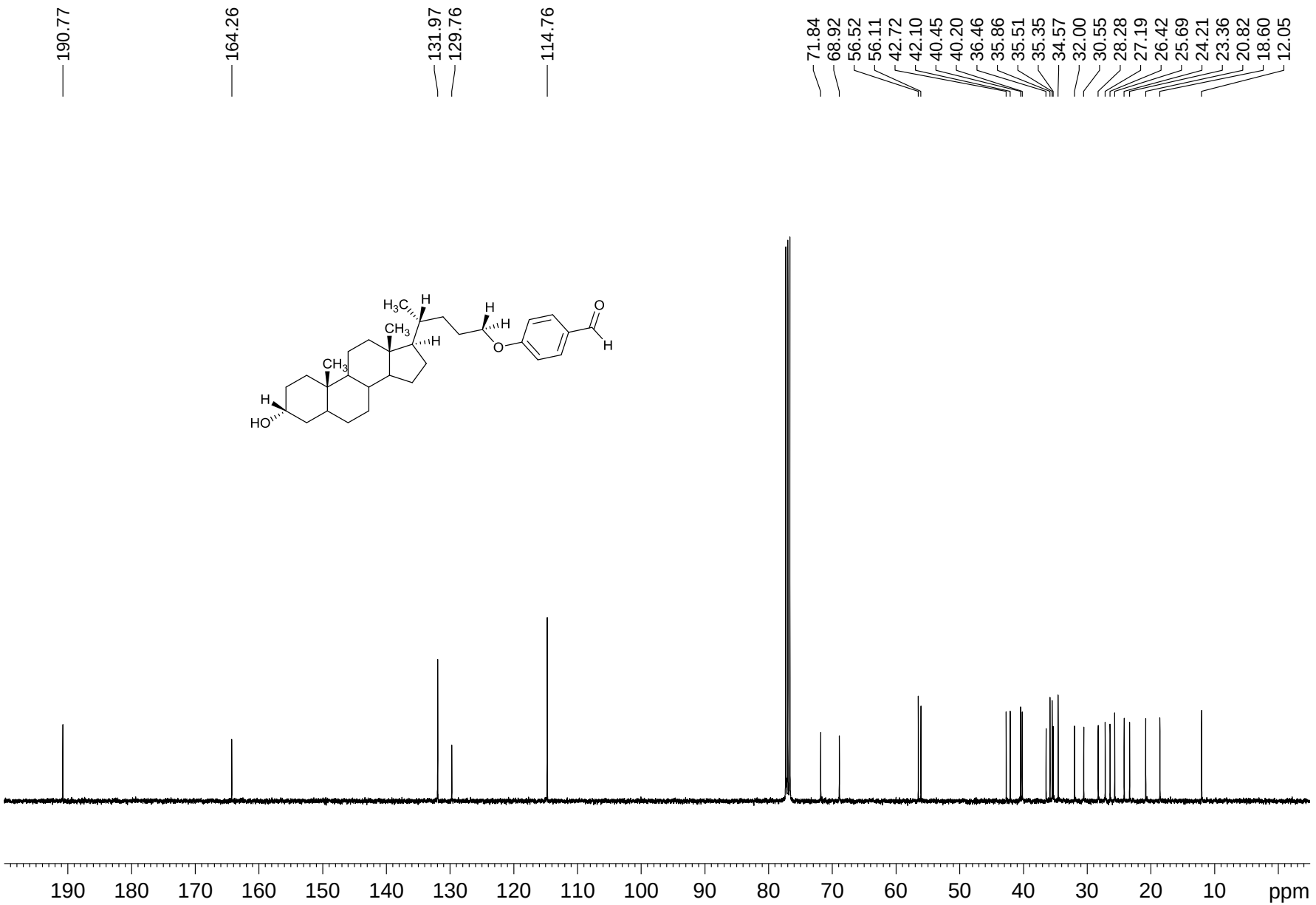

Fig. S23. ^{13}C NMR spectrum of **4** (100 MHz, $CDCl_3$).

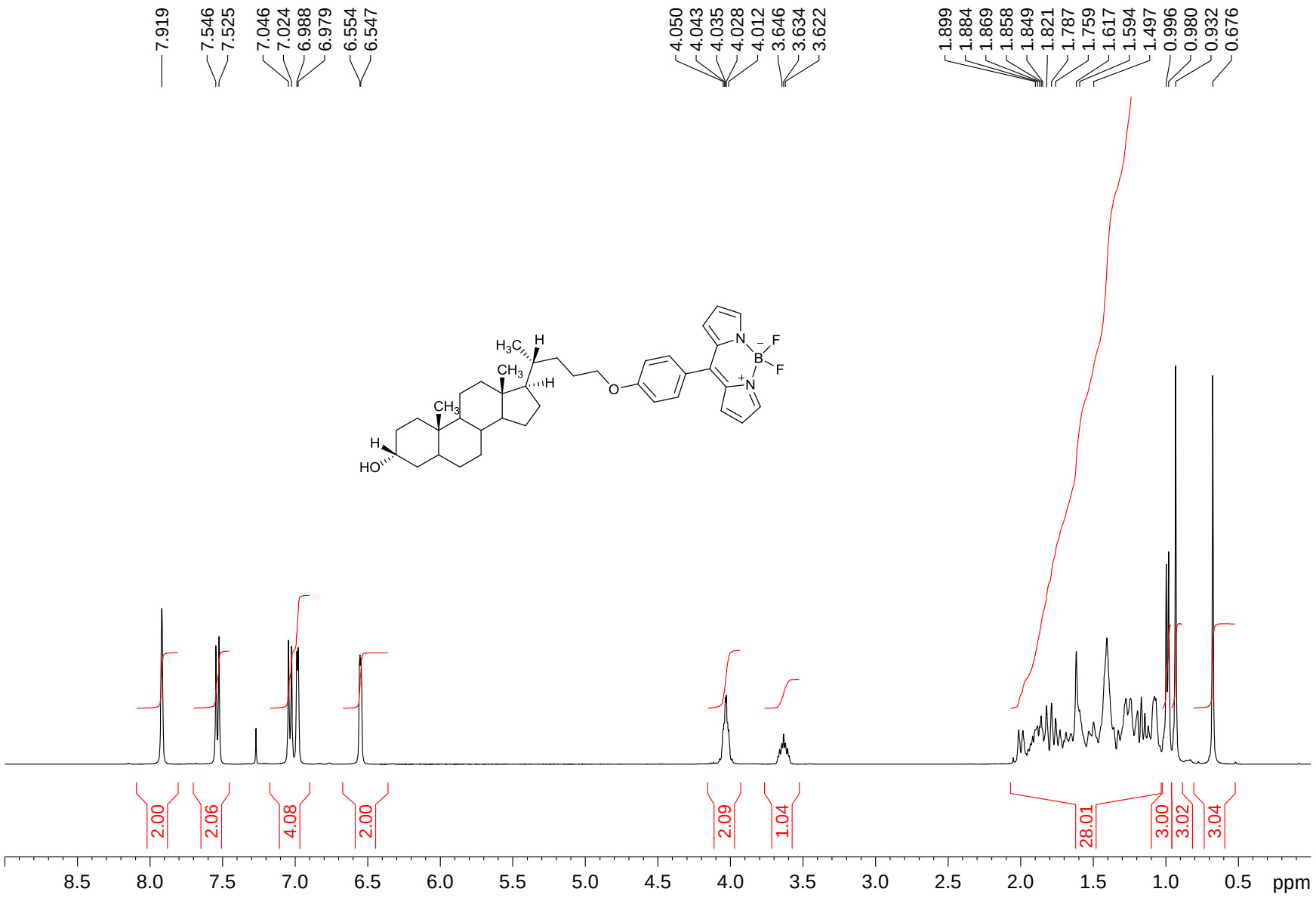

Fig. S24. ^{1}H NMR spectrum of rotor **3** (400 MHz, $CDCl_3$).

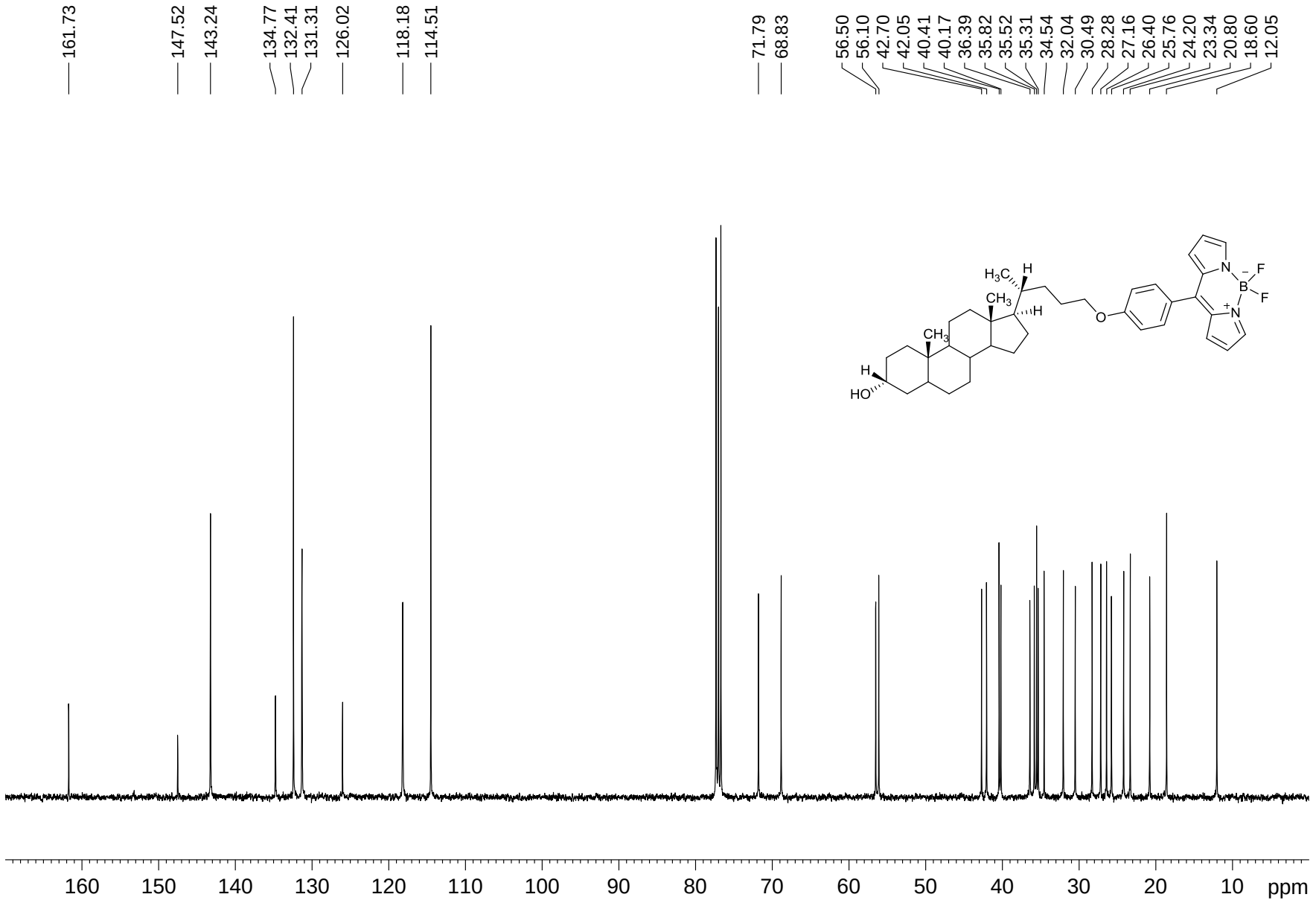

Fig. S25. ^{13}C NMR spectrum of rotor **3** (100 MHz, $CDCl_3$).

(7) References

1. Case, D.A., et al., *AMBER 12*, 2012: University of California, San Francisco.
2. Wang, J., et al., *Development and testing of a general amber force field.* Journal of Computational Chemistry, 2004. **25**: p. 1157-1174.
3. Bayly, C.I., et al., *A well-behaved electrostatic potential based method using charge restraints for deriving atomic charges: the RESP model.* The Journal of Physical Chemistry, 1993. **97**(40): p. 10269-10280.
4. Cornell, W.D., et al., *Application of RESP charges to calculate conformational energies, hydrogen bond energies, and free energies of solvation.* Journal of the American Chemical Society, 1993. **115**(21): p. 9620-9631.
5. Dickson, C.J., et al., *Lipid14: The Amber Lipid Force Field.* Journal of Chemical Theory and Computation, 2014. **10**(2): p. 865–879.
6. Jorgensen, W.L., et al., *Comparison of simple potential functions for simulating liquid water.* The Journal of Chemical Physics, 1983. **79**(2): p. 926-935.
7. Press, W.H., et al., *Numerical Recipes: The Art of Scientific Computing*. Third Edition ed2007, New York: Cambridge University Press.
8. Pastor, R., B. Brooks, and A. Szabo, *An analysis of the accuracy of Langevin and molecular dynamics algorithms.* Molecular Physics, 1988. **65**(6): p. 1409-1419.
9. Berendsen, H.J.C., et al., *Molecular dynamics with coupling to an external bath.* The Journal of Chemical Physics, 1984. **81**(8): p. 3684-3690.
10. Götz, A.W., et al., *Routine Microsecond Molecular Dynamics Simulations with AMBER on GPUs. 1. Generalized Born.* Journal of Chemical Theory and Computation, 2012. **8**(5): p. 1542-1555.
11. Salomon-Ferrer, R., et al., *Routine Microsecond Molecular Dynamics Simulations with AMBER on GPUs. 2. Explicit Solvent Particle Mesh Ewald.* Journal of Chemical Theory and Computation, 2013. **9**(9): p. 3878-3888.
12. Le Grand, S., A.W. Götz, and R.C. Walker, *SPFP: Speed without compromise—A mixed precision model for GPU accelerated molecular dynamics simulations.* Computer Physics Communications, 2013. **184**(2): p. 374-380.
13. Ryckaert, J.-P., G. Ciccotti, and H.J.C. Berendsen, *Numerical integration of the cartesian equations of motion of a system with constraints: molecular dynamics of n-alkanes.* Journal of Computational Physics, 1977. **23**(3): p. 327-341.

14. Roe, D.R. and T.E. Cheatham, *PTRAJ and CPPTRAJ: Software for Processing and Analysis of Molecular Dynamics Trajectory Data.* Journal of Chemical Theory and Computation, 2013. **9**(7): p. 3084-3095.

15. Anézo, C., et al., *Methodological Issues in Lipid Bilayer Simulations.* The Journal of Physical Chemistry B, 2003. **107**(35): p. 9424-9433.

16. Wu, Y. et al*., Molecular Rheometry: direct determination of viscosity in Lo and Ld lipid phases via fluorescence lifetime imaging*. Physical Chemistry Chemistry Physics, 2013, **15**, 14986-14993

17. López-Duarte, I. et al*., A molecular rotor for measuring viscosity in plasma membranes of live cells*, Chemical Communications, 2014, **50**, 5282-5284

18. Korson, L. et al., *Viscosity of water at various temperatures*, Journal of Physical Chemistry, 1969, **73**, 34-39

19. Bezlyepkina, N. et al., *Phase diagram and tie-line determination for the ternary mixture DOPC/eSM/Cholesterol*, Biophysical Journal, 2013, **104**, 1456-1464